Heterosynaptic GABAergic plasticity bidirectionally driven by the activity of pre- and postsynaptic NMDA receptors

Jonathan Mapelli[a,1], Daniela Gandolfi[a], Antonietta Vilella[a], Michele Zoli[a], and Albertino Bigiani[a]

[a]Dipartimento di Scienze Biomediche, Metaboliche e Neuroscienze, Center for Neuroscience and Neurotechnology, Università di Modena e Reggio Emilia, 41125 Modena, Italy

Edited by Gina G. Turrigiano, Brandeis University, Waltham, MA, and approved July 1, 2016 (received for review January 22, 2016)

Dynamic changes of the strength of inhibitory synapses play a crucial role in processing neural information and in balancing network activity. Here, we report that the efficacy of GABAergic connections between Golgi cells and granule cells in the cerebellum is persistently altered by the activity of glutamatergic synapses. This form of plasticity is heterosynaptic and is expressed as an increase (long-term potentiation, LTP_{GABA}) or a decrease (long-term depression, LTD_{GABA}) of neurotransmitter release. LTP_{GABA} is induced by postsynaptic NMDA receptor activation, leading to calcium increase and retrograde diffusion of nitric oxide, whereas LTD_{GABA} depends on presynaptic NMDA receptor opening. The sign of plasticity is determined by the activation state of target granule and Golgi cells during the induction processes. By controlling the timing of spikes emitted by granule cells, this form of bidirectional plasticity provides a dynamic control of the granular layer encoding capacity.

inhibitory plasticity | heterosynaptic plasticity | cerebellum | GABA | NMDA

Inhibitory neurotransmission regulates the stability of neuronal circuits by tuning, timing, gain, and excitability of principal neurons (1, 2). In turn, the efficacy of inhibitory synapses can be regulated by long-term potentiation (LTP) or depression (LTD) (3). Inhibitory plasticity participates in the maintenance of circuit stability and circuit refinement by shaping the dynamic range of excitatory neurons (4). At the molecular level, a broad spectrum of mechanisms can activate inhibitory plasticity (5–8). Among these mechanisms, the diffusion of nitric oxide (NO) following postsynaptic NMDA receptor ($NMDA_R$) opening was shown to mediate LTP (9). Conversely, circuit disinhibition through GABAegic LTD has been observed to be promoted by presynaptic $NMDA_R$s (10). However, the coexistence in the same synapse of potentiation and depression engaged by NMDA signaling has never been reported yet. The cerebellum coordinates sensory–motor function via the firing patterns of Purkinje cells (PCs), which are in turn modulated by the granular layer activity. Recent findings highlighted the role of single granule cells (GrCs) in processing cerebellar signals during locomotion, motor coordination, and sensory–motor integration (11, 12). Furthermore, the local computation in the granular layer is under control of Golgi cell (GoC) inhibitory activity through feedback and feedforward loops (13). GABAergic inhibition in fact regulates GrC output gain (14) and allows the tuning of first spike delay and precision (15) by implementing "time-windowing" operations (4). In addition, plastic mechanisms residing throughout the granular layer circuit are likely involved in shaping neural code. Among these mechanisms, the high-frequency discharge of mossy fibers (mfs) repeated in θ-rhythms potentiates glutamate release at the mf–GrC synapse through retrograde diffusion of NO (16). Here, we examined how a θ-burst stimulation (TBS) delivered to glutamatergic mfs influences the strength of neighboring GABAergic contacts. We found that GABAergic LTP (LTP_{GABA}) and LTD (LTD_{GABA}), which are engaged by NMDA signaling, modulate GrC firing and excitability, controlling signal processing in the granular layer.

Results

TBS Persistently Alters Inhibitory Neurotransmission in the Cerebellum Granular Layer. The mfs of the cerebellum convey information through bursts of high-frequency action potentials (17). These bursts can be organized in θ-band rhythm during specific tasks, such as spatial exploration (18), or synchronized to other brain regions during associative learning (19). θ-Burst activity was shown to induce glutamatergic LTP (LTP_{glu}) in vitro and in vivo (20, 21). Because synaptic inhibition impacts LTP_{glu} (21, 22), we investigated how TBS affected GrC firing in the presence of ongoing inhibition. Changes in GrC firing were monitored in current clamp configuration. The expression of LTP_{glu} was monitored by recording excitatory postsynaptic currents (EPSCs) elicited by paired pulse protocol in voltage clamp at −70 mV (Fig. 1*A*). We initially evaluated the effects of TBS in cells responding with suprathreshold activity to a single impulse delivered to the mf bundle (Fig. S1*A*). In 6 of 10 recorded cells, TBS delivered in current clamp configuration induced a marked LTP_{glu} (15) (+42.6 ± 4.3%, $n = 6$, $P < 0.01$) (Fig. 1*A*). As expected in response to the expression of LTP_{glu} (22), these cells showed a decrease of first spike latency together with an increase of first spike precision and of the probability of eliciting spikes (Fig. 1 *B* and *C*). Unexpectedly, in these GrCs, we observed a decrease in the number of spike doublets (Fig. 1 *B* and *C*). In the remaining GrCs, TBS was unable to induce LTP_{glu} (EPSCs +4.6 ± 6.1%, $n = 4$ cells, $P > 0.3$) (Fig. 1*D*). Interestingly, these cells showed a marked increase of spike doublets (Fig. 1 *E* and *F*) and a nonsignificant increase of probability of firing, whereas first spike delay and first spike precision were not altered (Fig. 1 *E* and *F*). Similarly, we analyzed GrCs showing subthreshold activity in response to single mf impulses.

Significance

The plasticity of inhibitory synapses is involved in regulating the balance between excitation and inhibition. Although a wide range of plastic mechanisms was analyzed in GABAergic synapses, a bidirectional plasticity engaged by NMDA signaling has never been observed. We report here that the synapse between Golgi cells and granule cells in the cerebellar granular layer can be modulated by heterosynaptic plasticity in a bidirectional manner, depending on NMDA receptors. Long-term potentiation is expressed in response to postsynaptic $NMDA_R$ activation via nitric oxide retrograde diffusion. Conversely, long-term depression is triggered by presynaptic $NMDA_R$ activation. The present results provide a plastic mechanism controlling signal processing in neural networks.

Author contributions: J.M. and D.G. designed research; J.M., D.G., and A.V. performed research; J.M., D.G., A.V., and M.Z. analyzed data; and J.M., M.Z., and A.B. wrote the paper.

The authors declare no conflict of interest.

This article is a PNAS Direct Submission.

[1]To whom correspondence should be addressed. Email: jonathan.mapelli@unimore.it.

This article contains supporting information online at www.pnas.org/lookup/suppl/doi:10.1073/pnas.1601194113/-/DCSupplemental.

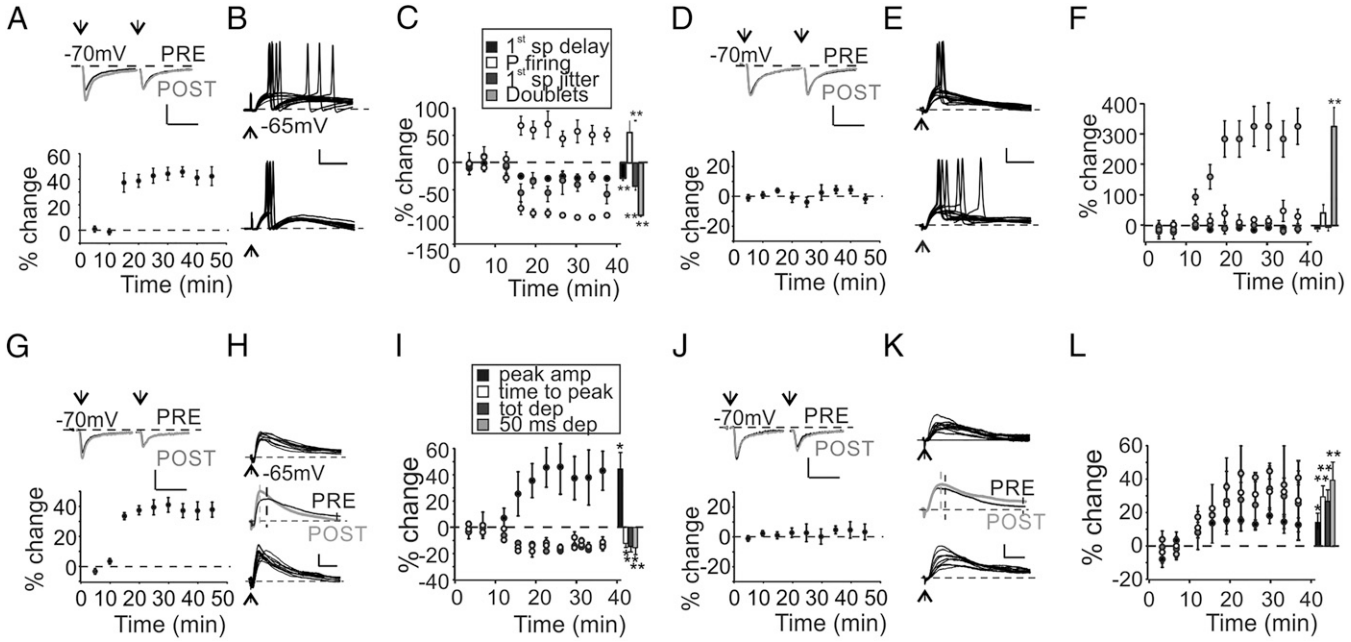

Fig. 1. Impact of TBS on GrC activity. (*A*, *Upper*) Average EPSCs obtained before (black) and after (gray) TBS in a GrC undergoing LTP_{glu}. (Scale bar: 10 ms, 20 pA.) (*Lower*) Time course of normalized EPSC changes ($n = 6$). (*B*) Voltage traces taken from the same GrC shown in *A* and generating suprathreshold responses following a single mf impulse before (*Upper*) and after (*Lower*) TBS. (Scale bar: 10 ms, 20 mV.) (*C*) Time course of spike-related parameters. Histogram summarizes average changes in cells undergoing LTP_{glu} (first spike delay −28.4 ± 4.3%, $^{**}P < 0.01$; first spike SD −43.4 ± 7.2%, $^{**}P < 0.01$; *P* firing +53.5 ± 19.4%, $^{**}P < 0.01$; doublets −95.7 ± 2.3%, $^{**}P < 0.01$, $n = 6$ cells). (*D*, *Upper*) Average EPSCs obtained before (black) and after (gray) TBS in a GrC in which LTP_{glu} was not expressed. (Scale bar: 10 ms, 20 pA.) (*Lower*) Time course of normalized EPSC changes ($n = 4$). (*E*) Voltage traces taken from the same GrC shown in *D*. (Scale bar: 10 ms, 20 mV.) (*F*) Time course of spike-related parameters. Histogram summarizes average changes in cells in which LTP_{glu} was not expressed (first spike delay −8.3 ± 3.3%, $P > 0.1$; first spike SD +4.5 ± 15.4%, $P > 0.9$; *P* firing +40.9 ± 22.7%, $P < 0.08$; doublets +322.2 ± 57.2%, $^{**}P < 0.01$, $n = 4$ cells). (*G*, *Upper*) Average EPSCs obtained before (black) and after (gray) TBS in a GrC undergoing LTP_{glu} and showing subthreshold activity in response to a single mf impulse. (Scale bar: 10 ms, 10 pA.) (*Lower*) Time course of normalized EPSC changes ($n = 5$). (*H*) Voltage traces taken from the same GrC shown in *G* before (*Upper*) and after (*Lower*) TBS. (Scale bar: 10 ms, 5 mV.) (*I*) Time course of EPSP-related parameters. Histogram summarizes average changes on EPSP properties in cells undergoing LTP_{glu} [peak amp +45.3 ± 11.1%, $^{*}P < 0.05$; time to peak −12.8 ± 2.5%, $^{*}P < 0.05$; total depolarization (tot dep) −14.9 ± 2.4%, $^{**}P < 0.01$; depolarization at 50 ms poststimulus (50 ms dep) −16.6 ± 4.2%, $^{**}P < 0.01$, $n = 5$ cells]. (*J*, *Upper*) Average EPSCs obtained before (black) and after (gray) TBS in a GrC in which LTP_{glu} was not expressed and showing subthreshold activity in response to a single mf impulse. (Scale bar: 10 ms, 10 pA.) (*Lower*) Time course of normalized EPSC changes ($n = 5$). (*K*) Voltage traces taken from the same GrC shown in *J*. (Scale bar: 10 ms, 5 mV.) (*L*) Time course of EPSP-related parameters. Histogram summarizes average changes on EPSP properties in cells in which LTP_{glu} was not expressed (peak amplitude +13.9 ± 6.4%, $^{*}P < 0.05$; time to peak +29.7 ± 9.1%, $^{**}P < 0.01$; tot dep 26.8 ± 6.8%, $^{**}P < 0.01$; 50 ms dep +39.5 ± 10.3%, $^{**}P < 0.01$, $n = 6$ cells).

Excitatory postsynaptic potentials (EPSPs) had an average time to peak of 7.9 ± 0.7 ms and a variable residual depolarization persisting for tens of milliseconds. A total of 5 of 11 cells showed LTP_{glu} (EPSCs +38.4 ± 6.1%, $n = 5$ cells, $P < 0.01$) (Fig. 1*G*). Accordingly, EPSPs showed amplitude increase and time-to-peak decrease (Fig. 1 *H* and *I*, see also ref. 22). In addition, despite the expression of LTP_{glu}, these cells exhibited a decrease of the total and residual depolarization (Fig. 1 *H* and *I*). In the remaining 6 cells, although EPSCs were unchanged (peak 3.8 ± 5.9%, $n = 6$ cells, $P > 0.4$) (Fig. 1*J*), TBS favored a small increase of all of the EPSP-related parameters (Fig. 1 *K* and *L*). To understand the origin of unexpected changes induced by TBS, we correlated values of spike- and EPSP-related parameters measured before TBS with the amount of glutamatergic potentiation. Cells undergoing LTP_{glu} initially showed higher probability of firing together with a larger number of spike doublets (Fig. S1*B*). Moreover, we observed a positive correlation between LTP_{glu} and EPSP amplitude and residual depolarization (Fig. S1*D*). Conversely, first spike jitter and delay poorly correlated with the amount of LTP_{glu} expressed (Fig. S1*C*). Because EPSCs evoked in cells expressing LTP_{glu} were not significantly different from the ones detected in nonpotentiated cells (47.2 ± 6.6 pA LTP_{glu} vs. 43.7 ± 7.3 pA non-LTP_{glu} for spiking cells, $P > 0.8$, 19.3 ± 2.9 pA LTP_{glu} vs. 18.1 ± 3.1 pA non-LTP_{glu} for nonspiking cells, $P > 0.7$), we hypothesized that excitatory inputs were similar among tested GrCs. We therefore speculated that diversities in inhibitory rather than excitatory inputs could produce the unexpected changes induced by TBS. We analyzed how the progressive reduction of GABAergic inhibition by SR9519 (gabazine) affected GrC responses. An increasing concentration of gabazine markedly enhanced the probability of firing and the number of doublets (Fig. S1 *E* and *F*), whereas poorly affecting first spike delay and jitter. Furthermore, gabazine increased EPSP amplitude and total and residual depolarization (Fig. S1 *G* and *H*). We concluded that parameters unexpectedly altered by TBS were tightly dependent on the amount of GABAergic inhibition. This evidence led us to hypothesize that besides LTP_{glu}, TBS could also alter the strength of inhibitory synapses.

LTP at GoCs–GrCs Is Heterosynaptic and Does Not Require GABAergic Activity. To investigate long-term plasticity at the inhibitory connections between GoCs and GrCs, we simultaneously activated GoC axons and mf terminals (Fig. S2*A*). We initially evoked EPSCs, which showed properties compatible with the ones elicited by direct mf stimulation (Fig. S2 *B* and *C*, *i*). Inhibitory postsynaptic currents (IPSCs) were then isolated by voltage clamping GrCs at 0 mV (Fig. S2 *C*, *ii*). The block of rapid AMPA glutamatergic currents by 20 μM 2,3-dihydroxy-6-nitro-7-sulfamoyl-benzo[f]quinoxaline-2,3-dione (NBQX) allowed to unmask monosynaptic evoked IPSCs (eIPSCs) showing faster kinetics (Fig. S2 *C*, *iii*) than polysynaptic eIPSCs. The application of TBS while holding GrCs at −40mV to release the intracellular magnesium from NMDA channels (Fig. S2 *C*, *iv* and *Materials and Methods*) induced a marked increase of eIPSC first peak amplitude (Fig. 2*A* and Fig. S2 *C*, *v*). This potentiation persisted for up to 40 min after the induction (Fig. 2*B*). The increase of

GABAergic currents was associated with a decrease of response variability [coefficient of variation (CV)] (*Materials and Methods* and Fig. S2*C*) and of paired pulse ratio (PPR) (Fig. S2*D*). On average, LTP_{GABA} was expressed as a persistent increase of eIPSC peak amplitude (+53.6 ± 7.3%, $n = 19$, $P < 0.001$) (Fig. 2*B*) together with a decrease of PPR (−20.2 ± 4.4%, $n = 19$, $P < 0.001$) (Fig. S2*D*) and of response CV (−29.6 ± 5.9%, $n = 19$, $P < 0.001$) (Fig. S2*E*). Notably, in 5 of 19 cells, after NBQX washout, GrC voltage clamp conditions allowed unmasking of a potentiation of EPSCs (+17.5 ± 1.8%, $n = 5$, $P < 0.01$), suggesting the concomitant expression of LTP_{glu} at the neighboring mf–GrC synapse. Besides changes of evoked currents, TBS induced an increase of spontaneous currents (sIPSCs) (Fig. S3*A*) elicited by the endogenous activity of GoCs (23). Furthermore, the frequency of sIPSC occurrence was unaffected (Fig. S3*A*), suggesting an increase of neurotransmitter release. The analysis of IPSC kinetics, revealed an increase of IPSC decay (Fig. S3*A*), indicating that alterations of postsynaptic receptor activity could not be ruled out. Moreover, the initial IPSC amplitude correlated with the initial EPSC amplitude ($R^2 = 0.79$, $n = 22$). Furthermore, in cells undergoing LTP_{GABA} (19 of 22; 86%), the amount of potentiation was proportional to the intensity of initial responses for both IPSCs ($R^2 = 0.82$) (Fig. S3*B*) and EPSCs ($R^2 = 0.85$) (Fig. S3*B*). Instead, in 3 of 22 cells (14%), TBS induced no significant changes, likely reflecting the absence of plasticity or, alternatively, the existence of compensatory mechanisms. A fundamental role in GrC neurotransmission is played by the tonic component of GABAergic inhibition, which is mediated by high-affinity extrasynaptic $GABA_A$ receptors, activated by persistent GABA concentrations in the glomerulus (24). We thus investigated whether LTP_{GABA} also affected the tonic component of inhibition. The expression of LTP_{GABA} was not accompanied by changes in holding currents (1.9 ± 2.5%, $n = 18$ cells, $P > 0.4$) (Fig. S3*C*) or in peak-to-peak noise of the holding current (0.5 ± 1.3%, $n = 18$ cells, $P > 0.4$) (Fig. S3*C*), indicating that the tonic component was not affected by LTP_{GABA}. We then investigated whether the induction of LTP_{GABA} depended on the activity of excitatory synapses. When electrical stimulation did not elicit glutamatergic currents, LTP_{GABA} was not observed (six of six cells) (Fig. S3*D*), suggesting the importance of glutamate in the induction of GABAergic potentiation. Given its dependence on glutamatergic activity, we asked whether LTP_{GABA} also depended on GABAergic activity. The TBS was therefore delivered in the presence of 20 μM gabazine, whose transient application reversibly blocked spontaneous and evoked currents, confirming their GABAergic origin (Fig. 2*C*). Following drug washout, IPSCs recovered to potentiated levels (+84.1 ± 16.8%, $n = 7$, $P < 0.01$) (Fig. 2 *C* and *D*), demonstrating the heterosynaptic nature of LTP_{GABA}. A marked decrease of PPR and CV (Fig. S4 *A* and *B*) was also measured. Different types of glutamatergic signaling have been shown to mediate GABAergic LTP in other brain structures. We hypothesized that the opening of $NMDA_{RS}$ during TBS-dependent depolarization could trigger intracellular Ca^{2+} increase, in turn inducing LTP_{GABA}. Recordings performed in the presence of 50 μM D-(-)-2-Amino-5-phosphonopentanoic acid (D-APV) indeed showed that IPSCs were not altered by TBS (−2.6 ± 3.5%, $n = 5$, $P > 0.5$) (Fig. 2 *E* and *F*), confirming that LTP_{GABA} was critically dependent on $NMDA_R$ activity.

The postsynaptic induction of LTP_{GABA} through a presynaptic maintenance mechanism requires the diffusion of a retrograde messenger potentiating GABA release. We investigated NO as a possible mediator of LTP_{GABA}. Recordings performed in slices preincubated and continuously perfused with the nitric oxide synthase (NOS) inhibitor, N^{ω}-nitro-L-arginine methyl ester hydrochloride (L-NAME) showed a complete block of LTP_{GABA} (Fig. 3*A*). Unexpectedly, IPSCs showed a significant and persistent peak amplitude decrease (-21.3 ± 4.1%; $n = 7$, $P < 0.05$) (Fig. 3*B*) along with an increase in the PPR and CV (Fig. S4 *C* and *D*). We termed this persistent depression in the efficacy of the GoC–GrC synapse LTD_{GABA}. To confirm the postsynaptic origin of LTP_{GABA} induction, we performed recordings with a high Ca^{2+} buffer concentration in the intracellular solution (10 mM BAPTA). LTP_{GABA} was blocked by 1,2-bis(2-aminophenoxy)ethane-N,N,N′,N′-tetraacetic acid (BAPTA) and IPSCs indeed showed depression (Fig. 3*B*) together with a persistent increase of PPR and CV (Fig. S4 *E* and *F*). These data confirmed that NO originated in the postsynaptic compartment following calcium entry through $NMDA_{RS}$. The guanylate cyclase (GC) and the subsequent cGMP activation are the main targets of NO. We therefore investigated the NO pathway by inhibiting GC with 5 μM 1H-[1,2,4]Oxadiazolo[4,3-a]quinoxalin-1-one (ODQ). Recordings performed on slices preincubated and continuously perfused with ODQ still showed a depression of IPSCs (Fig. 3*C*) and an increase of PPR and CV (Fig. S4 *E* and *F*). Accordingly, the perfusion of the membrane permeant cyclic GMP (cGMP) analog 8p-CPT-cGMP (25 μM) starting 10 min before TBS and in the presence of D-APV throughout recordings increased IPSC amplitude (Fig. 3*C*) and decreased PPR and CV (Fig. S4 *E* and *F*). These findings confirmed our hypothesis on the role of NO signaling in the expression of LTP_{GABA}.

We then investigated the mechanisms leading to LTD_{GABA}. The activation of metabotropic $GABA_B$ receptors in response to a 100-Hz train of GoC action potentials is known to transiently depress GABA release. Recordings performed in the presence of the $GABA_B$ receptor antagonist (2S)-3-[[(1S)-1-(3,4-Dichlorophenyl)ethyl]amino-2-hydro xypropyl](phenylmethyl)-phosphinic acid hydrochloride (CGP) together with L-NAME showed that, in response to a TBS at −40 mV, IPSCs were

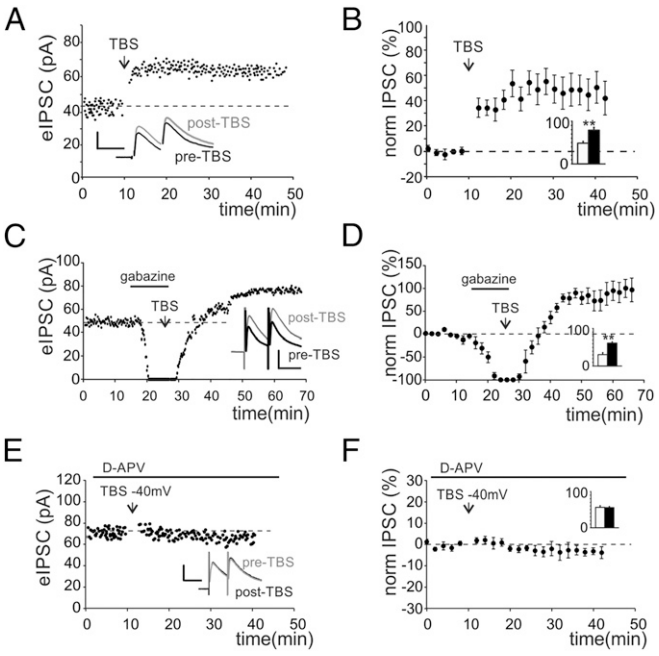

Fig. 2. TBS potentiates the activity of GoC–GrC synapses. (*A*) Time course of IPSC first peak amplitude in a single GrC. Traces in the *Inset* show average responses before (black) and after (gray) TBS. (Scale bar: 30 pA, 20 ms.) (*B*) Time course of normalized IPSC changes ($n = 19$). Histogram shows average IPSC values before (white) and after (black) TBS (50.1 ± 8.3 pA vs. 80.5 ± 9.7 pA $n = 19$, $^{**}P < 0.01$). (*C*) Time course of IPSCs first peak amplitude in a GrC transiently perfused with gabazine. TBS was delivered during gabazine perfusion (horizontal bar). Traces in the *Inset* show average responses before (black) and after (gray) TBS. (Scale bar: 40 pA, 20 ms.) (*D*) Time course of normalized IPSC changes in cells transiently perfused with gabazine ($n = 7$). Histogram shows average IPSC values (34.2 ± 2.6 pA vs. 62.1 ± 4.7 pA $n = 7$, $^{**}P < 0.01$). (*E*) Time course of IPSCs first peak amplitude in a GrC perfused with D-APV (horizontal bar). Traces in the *Inset* show average responses before (black) and after (gray) TBS. (Scale bar: 40 pA, 20 ms.) (*F*) Time course of normalized IPSCs changes ($n = 5$ cells) obtained from cells perfused with D-APV. Histogram shows average IPSC values (56.4 ± 3.5 pA vs. 54.8 ± 3.9 pA $n = 5$, $P > 0.6$).

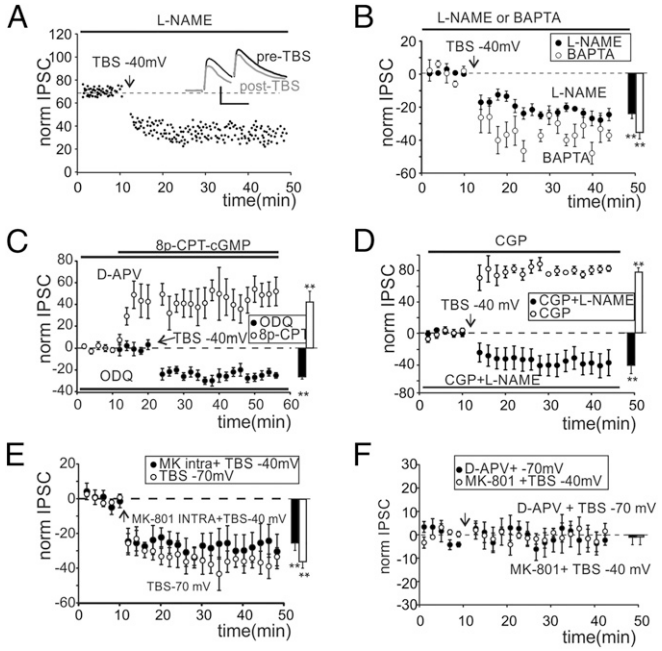

Fig. 3. Properties of LTP_{GABA} and LTD_{GABA}. (*A*) Time course of IPSCs first peak amplitude in a GrC incubated and perfused with L-NAME (horizontal bar). Traces in the *Inset* show average responses before (black) and after (gray) TBS. (Scale bar: 40 pA, 20 ms.) (*B*) Time course of normalized IPSC changes obtained from cells incubated and perfused with L-NAME (●) and cells recorded with high intracellular BAPTA (○). Histogram shows average IPSC changes (● −21.9 ± 3.9%, $n = 7$, $^{**}P < 0.01$; ○ −37.1 ± 4.3%, $n = 4$, $^{**}P < 0.01$). (*C*) Time course of normalized IPSC changes obtained from cells incubated (more than 2 h) and perfused with ODQ (●) and cells incubated and perfused with D-APV and transiently perfused with 8p-CPT-cGMP (○). Histogram shows average IPSC changes (● −24.7 ± 2.2%, $n = 4$, $^{**}P < 0.01$; ○ +41.5 ± 13.4%, $n = 4$, $^{**}P < 0.01$). (*D*) Time course of normalized IPSC changes obtained from cells perfused with CGP and L-NAME (●) and cells perfused with only CGP (○). Histogram shows average IPSC changes (● −44.1 ± 10.4%, $n = 5$, $P < 0.01$; ○ +78.4 ± 3.1%, $n = 5$, $P < 0.01$). (*E*) Time course of normalized IPSC changes obtained from cells with intracellular MK-801 (●) and cells receiving TBS at −70 mV (○). Histogram shows average IPSC changes (● −25.5 ± 6.1%, $n = 5$, $^{**}P < 0.01$; ○ −35.9 ± 10.3%, $n = 6$, $^{**}P < 0.01$) (*F*) Time course of normalized IPSC changes obtained with TBS at −70 mV and in the presence of D-APV (●) and cells with extracellular MK-801 and TBS at −40 mV (○). Histogram shows average IPSC changes (● −1.3 ± 4.2%, $n = 5$, $P > 0.7$; ○ −1.1 ± 3.7%, $n = 4$, $P > 0.6$).

persistently depressed (Fig. 3*D*), whereas PPR and CV were increased (Fig. S4 *E* and *F*). Furthermore, the presence of the sole CGP in the bath solution still showed IPSC depression (Fig. 3*D*) along with PPR and CV increase (Fig. S4 *E* and *F*). These data indicated that $GABA_B$ receptors were not involved in the induction of both forms of plasticity. The evidence that, in the presence of D-APV, IPSCs were unchanged (Fig. 2 *E* and *F*) led us to hypothesize that $NMDA_R$s could be involved in the induction of LTD_{GABA}. Extrasynaptic $NMDA_R$s were in fact shown to mediate some forms of long-term plasticity in central synapses (25). Similarly, we supposed that presynaptic $NMDA_R$s could be involved in the induction of LTD_{GABA}. TBS was therefore delivered while holding GrCs at −70 mV to limit the contribution of postsynaptic $NMDA_R$s by virtue of the voltage-dependent Mg^{2+} block. LTP_{GABA} was indeed converted into LTD_{GABA} (Fig. 3*E*), whereas PPR and CV were increased (Fig. S4 *E* and *F*). Our hypothesis was confirmed by adding to the intracellular solution the NMDA ion channel blocker MK-801 (500 μM) to inhibit postsynaptic $NMDA_R$ opening. The depression of IPSCs (Fig. 3*E*) and the increase of PPR and CV (Fig. S4 *E* and *F*) demonstrated that postsynaptic $NMDA_R$s were essential to induce LTP_{GABA}, leaving space for a role of presynaptic $NMDA_R$s in the induction of LTD_{GABA}. When TBS was delivered at −70 mV and in the presence of D-APV, IPSC depression was abolished (Fig. 3*F*). Furthermore, a metabotropic NMDA-dependent pathway has been shown to mediate hippocampal LTP (26). Thus, 100 μM (5S,10R)-(+)-5-methyl-10,11-dihydro-5H-dibenzo[a,d]cyclohepten-5,10-imine maleate (MK-801) was added to the extracellular solution to block ion influx through NMDA channels while delivering TBS at −40 mV. Recordings performed on slices preincubated and continuously perfused with MK-801 showed that NMDA channel opening is essential to trigger both forms of plasticity (Fig. 3*F*). The effect of LTP_{GABA} and LTD_{GABA} on membrane potentials was evaluated by measuring inhibitory postsynaptic potential (IPSP) changes (Fig. S5 *A* and *B*). Because these variations may derive from a shift of the Cl^- reversal potential (27), IPSC amplitudes were measured while holding GrCs at a different membrane potential. No significant changes were observed between values obtained before and after TBS in both cases (Fig. S5*B*). This evidence confirmed that changes in IPSPs depended on potentiation and depression of GABA release.

Finally, GrC firing and subthreshold activity changes in response to TBS (Fig. 1) were evaluated when both LTP and LTD were abolished by D-APV. Both spike- and EPSP-related parameters were unaffected by TBS (Fig. S5 *C* and *D*), confirming that alterations on GrC response properties initially observed (Fig. 1) originated at least in part from GABAergic bidirectional plasticity.

In the classic view, $NMDA_R$s act postsynaptically to control excitatory neurotransmission. In the granular layer, dendritic $NMDA_R$s modulate glutamatergic neurotransmission from mf to both GrCs and GoCs. Our evidence on the induction of LTD_{GABA} implies the presence of presynaptic $NMDA_R$s on GoC axonal terminals, which were never observed. We thus performed triple immunostaining against NR1 $NMDA_R$ subunit (Fig. 4 *C*, *G*, *K*, and *O*), synaptophysin (Fig. 4 *B*, *F*, *J*, and *N*), and glutamic acid decarboxylase (GAD) (Fig. 4 *A*, *E*, *I*, and *M*) to identify $NMDA_R$s, presynaptic boutons, and GoCs, respectively. As expected, a few scattered immunoreactive GoCs were found in the granular layer, whereas synaptophysin immunoreactive synapses were found concentrated in the glomeruli (Fig. 4 *D*, *H*, *L*, and *P*). As previously reported (28), NR1 immunoreactivity was scattered across the granular layer and richly decorated the large synaptophysin immunoreactive spots of the glomeruli. To assess the presence of presynaptic $NMDA_R$s on GABAergic boutons of the

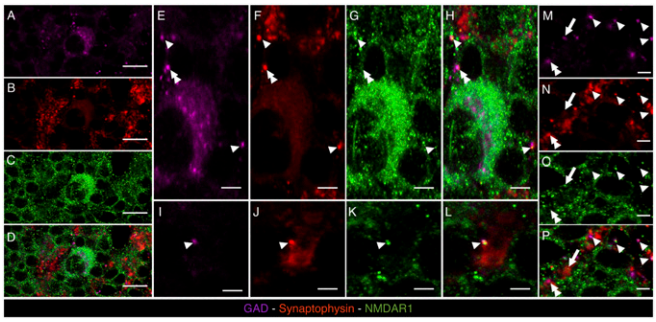

Fig. 4. Confocal microscopy images of brain cryosections labeled with mouse anti-GAD (magenta), guinea pig anti-synaptophysin (red), and rabbit anti-NR1 (green), of the granular cell layer of cerebellum. (*A–D*) A GAD^+ GoC (magenta, indicated in *A*) is represented, showing membrane staining for NR1 (green, *C*). (*E–H*) Magnifications of the GAD^+ cell represented in *A* showing single (red, green, or magenta pixels for synaptophysin, NR1, and GAD staining, respectively) or multiple labelings marked with different labels: arrowhead for triple colocalization of GAD, synaptophysin, and NR1 signals; double arrowhead for colocalization of GAD and synaptophysin signals; and arrow for colocalization of synaptophysin and NR1 signals. (*I–P*) Taken from granular layer neuropil, different spots with high degree of labeling colocalization are indicated using the same label code used in *E–H*. [Scale bars: 50 μm (*A–D*) and 15 μm (*E–P*).]

NEUROSCIENCE

granular layer, we singled out GAD/synaptophysin-stained structures of about 1 μm as putative GABAergic boutons and verified whether they were also stained for NR1 immunoreactivity. The analysis of 10 confocal images (70 × 70 μm, 1 μm thick) showed that roughly 80% (151/185) of putative GABAergic boutons express NR1 immunoreactivity (colocalization was considered positive when a NR1 immunoreactive spot was contained within a putative GABAergic bouton and covered ≥30% of its area). We also found several instances of ∼1-μm-thick structures positive for GAD and NR1 immunoreactivity but negative for synaptophysin that were interpreted as thin GABAergic dendritic processes of the GoCs or GABAergic axons of the Purkinje cells expressing postsynaptic $NMDA_R$s. As a negative control we performed triple immunostaining against NR1, synaptophysin, and gephyrin (a protein associated with $GABA_A$ receptors), and found no instances of triple colocalization of these markers in the granular layer (Fig. S6).

Discussion

We have shown a form of GABAergic heterosynaptic plasticity requiring the opening of pre- and postsynaptic $NMDA_R$s. We reached this conclusion by examining the induction mechanisms. First, the presence in the extracellular solution of D-APV or MK-801 prevented both forms of plasticity. Second, LTP_{GABA} could not be induced when postsynaptic $NMDA_R$s were blocked by GrC hyperpolarization, intracellular MK-801, or high concentration of Ca^{2+} buffer. Third, none of these conditions prevented the induction of LTD_{GABA}. Fourth, LTD_{GABA} was unmasked when presynaptic expression of LTP_{GABA} was inhibited by the block of NO synthesis and diffusion. We showed that this form of plasticity governs first spike precision and the number of spikes emitted by GrCs. The interplay between glutamatergic and GABAergic synapses dynamically controls GrC output patterns.

Bidirectional plasticity rules depending on glutamate receptors have been identified in GABAergic synapses of neonatal hippocampus (29) and in the basolateral amygdala (30). In these brain regions, the sign of plasticity depended on the ontogenetic developmental stage or, alternatively, on the activity of specific kainate receptor subtypes. Here, we describe a mechanism in which learning rules rather depended on the activation state of neurons involved in the induction processes [state-dependent plasticity, (SDP)]. The mechanisms underlying the sign of SDP are mediated by the activation of presynaptic and postsynaptic $NMDA_R$s, whose gating is influenced by the corresponding neuron. As in other areas, in the cerebellar granular layer, the excitatory/inhibitory ratio (*E*/*I*) originates from the reciprocal interaction of excitatory and inhibitory afferences (21). Similarly to what was recently observed in the hippocampus (31) and in the auditory cortex (32), cerebellar inhibitory SDP compensates unbalanced *E*/*I*, implementing a negative feedback control of neuronal activity. LTP_{GABA}, predominantly observed in poorly inhibited neurons (Fig. 1 *A* and *G*), limits hyperexcited states arising from the potentiation of the mf–GrC synapse (21). Conversely, in poorly excitable GrCs (Fig. 1 *D* and *J*), the initial disinhibition triggered by high-frequency activity and mediated by presynaptic metabotrobic glutamate receptors and $GABA_{BR}$ (33) can be reinforced by the expression of LTD_{GABA}. Central to these processes is the engagement of specific NMDA signaling. The role of GoCs in SDP induction is also important because (*i*) GoCs are spontaneously active at low frequency (23) and (*ii*) mf high-frequency discharge induces a firing reset in the refractory period (23). It is plausible that TBS is unable to induce a persistent depolarization capable of unblocking $NMDA_R$s located on presynaptic GoC terminals. Nevertheless, among NMDA subunits expressed by GoCs, the low conductance NR1/NR2D complex (*i*) is preferentially located extrasynaptically and poorly contributes to EPSCs, (*ii*) is insensitive to voltage-dependent Mg^{2+} block, and (*iii*) shows slow deactivation rates (34). LTD_{GABA} could thus be subtly sensitive to GoC activity, and glutamate diffusion following TBS tends to depress GABAergic activity. This depression can be indeed converted into potentiation by mechanisms triggered by NO diffusion. The GoC-mediated inhibition is a fundamental player in controlling the temporal coding in cerebellar circuitry. GoC inhibition was in fact shown to operate as gain controller of GrC excitation and regulator of the temporal fidelity of mf–GrC neurotransmission (11, 15, 17, 35).

Recent findings also showed that when sensory information is conveyed to GrCs, the temporal precision of excitatory neurotransmission is weakened by GoC synaptic inhibition in favor of an increased response reproducibility across the GrC population (11). Our results demonstrate that the excess of excitation generated by LTP_{glu} in poorly inhibited GrCs is compensated by LTP_{GABA} improving time windowing (4). As a whole, the interplay between LTP_{glu} and LTP_{GABA} leads to an enhanced first spike precision and to a reduction of the total amount of emitted spikes. The result is thus a more efficient and reliable neurotransmission. A reduced spike discharging poorly correlated with synaptic inputs could in fact lower the noise in the transmission of information (36). Conversely, LTD_{GABA} occurring when inhibition excessively dampens GrC membrane potential helps GrCs to approach firing regime and widening the time window for spike transmission. Furthermore, LTD_{GABA} could act on the total inhibitory strength by reducing spillover inhibition activated by parallel circuits (37). As a whole, heterosynaptic SDP could increase the overall capability of the system to modulate signal transfer (36, 38). The potentiation of GoC–GrC would in fact maximize the temporal precision of mf–GrC neurotransmission by narrowing time windowing, whereas the depression of GABAergic efficacy following LTD_{GABA} could facilitate temporal summation of excitatory inputs during repetitive neurotransmission.

Finally, GrCs were recently shown to integrate inputs coming from different sensory pathways and generating distinct firing patterns representative of multimodal input combinations (12). Long-term plastic mechanisms separately occurring in single dendrites could contribute to potentiate input specificity and classification. The GoC–GrC connectivity has inspired the hypothesis that GoC inhibition also controls the spatial patterns of granule cell activity. Bidirectional GABAergic plasticity could provide a spatial modulation of granular layer activity, which in the granular layer is organized in center-surround structures (21, 39, 40). The lipophilic nature of NO, by facilitating diffusion across cell membranes, would generate a wide sphere of influence (41). NO diffusion from cores of activation could potentiate GABAergic inhibition in surrounding regions thus sharpening center-surround structures (21, 39). In particular, the correlation between EPSCs and the amount of LTP_{GABA} (Fig. S3*B*) suggests that GrCs receiving stronger excitatory inputs produce a larger amount of NO to also be spread to nearby glomeruli, thus activating "silent" synapses (42). Conversely, by virtue of its inability to cross cell membranes, glutamate remains confined inside glomeruli. We can speculate that the sign of inhibitory plasticity depends on the balance between the inactivation rate of presynaptic $NMDA_R$s and NO (16). Experimental findings and theoretical predictions showed that the sphere of influence of NO from point sources has a limited radius (less than 100 μm) (41) and lasts for less than 1 s (16). These values are compatible with the size of the recently observed center-surround structures in the granular layer (21, 39, 40, 43). We can conclude that in response to heterosynaptic bidirectional SDP, GoC-mediated inhibition proportionally scales with excitatory input implementing a dynamic regulation of GrC responses (37). This form of heterosynaptic SDP provides an additional mechanism for the modulation of GrC response magnitude. A major contribution of this study is that we have demonstrated the existence of a form of bidirectional GABAergic plasticity dependent on the activity of neighboring glutamatergic synapses.

Materials and Methods

Experiments were performed by using Sprague-Dawley rats at postnatal days P17–P24 (internal breeding; Charles River Laboratories). All experiments were conducted in accordance with international guidelines from the European Community Council Directive 86/609/EEC on the ethical use of animals. Parasagittal cerebellar slices were obtained as described in ref. 40. Experiments were performed at 32 °C using the standard patch-clamp recording technique. Drugs were purchased from Tocris Bioscience and Sigma-Aldrich. All data are expressed as mean ± SEM.

Electrophysiological Recordings. Whole-cell recordings from GrCs were obtained with patch-clamp technique by using an Axopatch 200B amplifier (Molecular Devices). Patch pipettes were filled with the following solution (in millimoles): 126 K-gluconate, 8 NaCl, 15 glucose, 5 Hepes, 1 $MgSO_4$, 0.1 BAPTA-4K, 0.05 BAPTA-Ca^{2+}, 3 ATP, 100 μM GTP; pH adjusted to 7.2 with KOH. Simultaneous IPSCs and EPSCs were elicited by stimulating GoC axons and mf terminals through a bipolar tungsten electrode positioned in the granular layer close to the recorded GrC (Fig. S2*A*) (Clark Instruments; stimulation intensity ± 5–15 V, 100 μs). EPSP- and ESPS-spike complexes were elicited by positioning the bipolar electrode across the mf bundle (Fig. S1*A*). Paired pulse stimulation was generated at a frequency of 20 Hz and acquisition was repeated at 0.1-Hz repetition. The PPR was calculated as the ratio between the second and the first peak amplitude. The CV of IPSCs and EPSCs was calculated as the ratio between the SD and the average of 10 consecutive responses. Current relaxation induced by a 10-mV step from the holding potential was analyzed to ensure recording stability. The tonic inhibition was estimated by measuring the holding current recorded in voltage clamp configuration at 0 mV and the average noise peak to peak of the same holding current. GrCs showed average membrane capacitance (1.9 ± 0.4 pF, $n = 38$), input resistance (1.9 ± 0.1 GΩ, $n = 38$), and series resistance (17.3 ± 0.5 MΩ, $n = 38$). The induction of plasticity was estimated by evaluating changes between 10 min before TBS and a period of at least 20 min after TBS. Cells showing unstable responses or changes in series resistance larger than 20% throughout recordings were discarded. In current clamp configuration, GrCs had an average resting potential of −64.3 ± 0.7 mV ($n = 20$ cells), whereas EPSP potentials were generated starting from a membrane potential between −55 and −65 mV (−64.3 ± 0.7 mV, $n = 20$ cells). Spike- and EPSP-related parameters were calculated as follows: (*i*) first spike delay, (*ii*) first spike jitter (SD of the first spike latency), (*iii*) *P* firing (the number of times a GrC elicited at least one spike over 10 repetitions), (*iv*) spike doublets (number of times a GrC elicited two spikes over 10 repetitions), (*v*) EPSP time to peak, (*vi*) EPSP peak amplitude, (*vii*) EPSP total depolarization (integral of membrane depolarization between the onset and 50 ms from stimulus onset (44), and (*viii*) residual depolarization (difference between the membrane potential before stimulus and 50-ms poststimulus).

Immunofluorescence Analysis. For histological processing, rats were prepared as in ref. 45. Briefly, rats were anesthetized and perfused with 4% (wt/vol) paraformaldehyde. Brains were then dissected out, postfixed, and frozen. Coronal 50-μm-thick section series were cut at a cryotome. Brain sections were processed for multiple immunofluorescence histochemistry. Incubation with anti-NR1 (rabbit, a kind gift of Cecilia Gotti, CNR Neuroscience Institute, Milan), anti-GAD (mouse monoclonal, Millipore), anti-synaptophysin, (guinea pig, a kind gift of Andreas Grabrucker, University of Ulm, Germany), anti-gephyrin (mouse, Synaptic Systems) diluted in 0.3% Triton X-100, 1% normal serum, and PBS 1× was performed overnight. Incubation with secondary antibodies (Alexa Fluor anti-rabbit 488, Alexa Fluor anti-mouse, and 546 Alexa Fluor anti-guinea pig 633) was carried out for 9 min at room temperature. Finally, brain sections were placed on gelatinized glass slides, dried and, after incubation with DAPI, mounted for confocal microscopy analysis (Leica, VTZ2000).

ACKNOWLEDGMENTS. We thank Rita Bardoni for helpful discussions; Claudia Giannini for data analysis; and Giuseppina Leo and Letizia Manca for confocal image analysis. This work was supported by a grant of the Fondazione di Vignola (to J.M.).

1. Wehr M, Zador AM (2003) Balanced inhibition underlies tuning and sharpens spike timing in auditory cortex. *Nature* 426(6965):442–446.
2. Gabernet L, Jadhav SP, Feldman DE, Carandini M, Scanziani M (2005) Somatosensory integration controlled by dynamic thalamocortical feed-forward inhibition. *Neuron* 48(2): 315–327.
3. Maffei A, Nelson SB, Turrigiano GG (2004) Selective reconfiguration of layer 4 visual cortical circuitry by visual deprivation. *Nat Neurosci* 7(12):1353–1359.
4. Pouille F, Scanziani M (2001) Enforcement of temporal fidelity in pyramidal cells by somatic feed-forward inhibition. *Science* 293(5532):1159–1163.
5. Fenselau H, Heinke B, Sandkühler J (2011) Heterosynaptic long-term potentiation at GABAergic synapses of spinal lamina I neurons. *J Neurosci* 31(48):17383–17391.
6. Araque A, et al. (2014) Gliotransmitters travel in time and space. *Neuron* 81(4):728–739.
7. Castillo PE, Chiu CQ, Carroll RC (2011) Long-term plasticity at inhibitory synapses. *Curr Opin Neurobiol* 21(2):328–338.
8. Kullmann DM, Moreau AW, Bakiri Y, Nicholson E (2012) Plasticity of inhibition. *Neuron* 75(6):951–962.
9. Nugent FS, Penick EC, Kauer JA (2007) Opioids block long-term potentiation of inhibitory synapses. *Nature* 446(7139):1086–1090.
10. Lien CC, Mu Y, Vargas-Caballero M, Poo MM (2006) Visual stimuli-induced LTD of GABAergic synapses mediated by presynaptic NMDA receptors. *Nat Neurosci* 9(3):372–380.
11. Powell K, Mathy A, Duguid I, Häusser M (2015) Synaptic representation of locomotion in single cerebellar granule cells. *eLife* 4:e07290.
12. Chabrol FP, Arenz A, Wiechert MT, Margrie TW, DiGregorio DA (2015) Synaptic diversity enables temporal coding of coincident multisensory inputs in single neurons. *Nat Neurosci* 18(5):718–727.
13. Billings G, Piasini E, Lőrincz A, Nusser Z, Silver RA (2014) Network structure within the cerebellar input layer enables lossless sparse encoding. *Neuron* 83(4):960–974.
14. Rothman JS, Cathala L, Steuber V, Silver RA (2009) Synaptic depression enables neuronal gain control. *Nature* 457(7232):1015–1018.
15. Nieus T, et al. (2006) LTP regulates burst initiation and frequency at mossy fiber-granule cell synapses of rat cerebellum: Experimental observations and theoretical predictions. *J Neurophysiol* 95(2):686–699.
16. Maffei A, et al. (2003) NO enhances presynaptic currents during cerebellar mossy fiber-granule cell LTP. *J Neurophysiol* 90(4):2478–2483.
17. Chadderton P, Margrie TW, Häusser M (2004) Integration of quanta in cerebellar granule cells during sensory processing. *Nature* 428(6985):856–860.
18. Szwed M, Bagdasarian K, Ahissar E (2003) Encoding of vibrissal active touch. *Neuron* 40(3):621–630.
19. Hoffmann LC, Berry SD (2009) Cerebellar theta oscillations are synchronized during hippocampal theta-contingent trace conditioning. *Proc Natl Acad Sci USA* 106(50):21371–21376.
20. Roggeri L, Rivieccio B, Rossi P, D'Angelo E (2008) Tactile stimulation evokes long-term synaptic plasticity in the granular layer of cerebellum. *J Neurosci* 28(25):6354–6359.
21. Mapelli J, D'Angelo E (2007) The spatial organization of long-term synaptic plasticity at the input stage of cerebellum. *J Neurosci* 27(6):1285–1296.
22. Armano S, Rossi P, Taglietti V, D'Angelo E (2000) Long-term potentiation of intrinsic excitability at the mossy fiber-granule cell synapse of rat cerebellum. *J Neurosci* 20(14): 5208–5216.
23. Forti L, Cesana E, Mapelli J, D'Angelo E (2006) Ionic mechanisms of autorhythmic firing in rat cerebellar Golgi cells. *J Physiol* 574(Pt 3):711–729.
24. Brickley SG, Cull-Candy SG, Farrant M (1996) Development of a tonic form of synaptic inhibition in rat cerebellar granule cells resulting from persistent activation of GABAA receptors. *J Physiol* 497(Pt 3):753–759.
25. Duguid IC, Smart TG (2004) Retrograde activation of presynaptic NMDA receptors enhances GABA release at cerebellar interneuron-Purkinje cell synapses. *Nat Neurosci* 7(5):525–533.
26. Nabavi S, et al. (2013) Metabotropic NMDA receptor function is required for NMDA receptor-dependent long-term depression. *Proc Natl Acad Sci USA* 110(10):4027–4032.
27. Woodin MA, Ganguly K, Poo MM (2003) Coincident pre- and postsynaptic activity modifies GABAergic synapses by postsynaptic changes in Cl^- transporter activity. *Neuron* 39(5):807–820.
28. Petralia RS, Yokotani N, Wenthold RJ (1994) Light and electron microscope distribution of the NMDA receptor subunit NMDAR1 in the rat nervous system using a selective anti-peptide antibody. *J Neurosci* 14(2):667–696.
29. McLean HA, Caillard O, Ben-Ari Y, Gaiarsa JL (1996) Bidirectional plasticity expressed by GABAergic synapses in the neonatal rat hippocampus. *J Physiol* 496(Pt 2):471–477.
30. Braga MF, Aroniadou-Anderjaska V, Xie J, Li H (2003) Bidirectional modulation of GABA release by presynaptic glutamate receptor 5 kainate receptors in the basolateral amygdala. *J Neurosci* 23(2):442–452.
31. Hunt DL, Puente N, Grandes P, Castillo PE (2013) Bidirectional NMDA receptor plasticity controls CA3 output and heterosynaptic metaplasticity. *Nat Neurosci* 16(8):1049–1059.
32. Sun YJ, et al. (2010) Fine-tuning of pre-balanced excitation and inhibition during auditory cortical development. *Nature* 465(7300):927–931.
33. Mitchell SJ, Silver RA (2000) Glutamate spillover suppresses inhibition by activating presynaptic mGluRs. *Nature* 404(6777):498–502.
34. Monyer H, Burnashev N, Laurie DJ, Sakmann B, Seeburg PH (1994) Developmental and regional expression in the rat brain and functional properties of four NMDA receptors. *Neuron* 12(3):529–540.
35. Sargent PB, Saviane C, Nielsen TA, DiGregorio DA, Silver RA (2005) Rapid vesicular release, quantal variability, and spillover contribute to the precision and reliability of transmission at a glomerular synapse. *J Neurosci* 25(36):8173–8187.
36. Bialek W, Rieke F, de Ruyter van Steveninck RR, Warland D (1991) Reading a neural code. *Science* 252(5014):1854–1857.
37. Duguid I, et al. (2015) Control of cerebellar granule cell output by sensory-evoked Golgi cell inhibition. *Proc Natl Acad Sci USA* 112(42):13099–13104.
38. Borst A, Theunissen FE (1999) Information theory and neural coding. *Nat Neurosci* 2(11):947–957.
39. Gandolfi D, Mapelli J, D'Angelo E (2015) Long-term spatiotemporal reconfiguration of neuronal activity revealed by voltage-sensitive dye imaging in the cerebellar granular layer. *Neural Plast* 2015:284986.
40. Gandolfi D, et al. (2014) The spatiotemporal organization of cerebellar network activity resolved by two-photon imaging of multiple single neurons. *Front Cell Neurosci* 8:92.
41. Wood J, Garthwaite J (1994) Models of the diffusional spread of nitric oxide: Implications for neural nitric oxide signalling and its pharmacological properties. *Neuropharmacology* 33(11):1235–1244.
42. Bekkers JM (2005) Presynaptically silent GABA synapses in hippocampus. *J Neurosci* 25(16):4031–4039.
43. Mapelli J, Gandolfi D, D'Angelo E (2010) Combinatorial responses controlled by synaptic inhibition in the cerebellum granular layer. *J Neurophysiol* 103(1):250–261.
44. Mapelli J, et al. (2015) The effect of desflurane on neuronal communication at a central synapse. *PLoS One* 10(4):e0123534.
45. Vilella A, et al. (2014) Insight on the fate of CNS-targeted nanoparticles. Part I: Rab5-dependent cell-specific uptake and distribution. *J Control Release* 174:195–201.